Engineering Geology 358 (2025) 108422

Contents lists available at ScienceDirect

Engineering Geology

journal homepage: www.elsevier.com/locate/enggeo

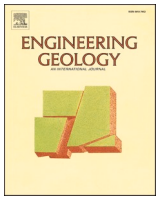

Mechanisms of river dam formation by debris flows highlighted through comparison with dry avalanches

Tianjia Zhou [a,b], Gordon G.D. Zhou [a,b,c,*], Kahlil F.E. Cui [a,b], Hongwei Luo [a,b], Xueqiang Lu [a,b], Alessandro Pasuto [d], Giulia Bossi [d]

[a] Key Laboratory of Mountain Hazards and Engineering Resilience / Institute of Mountain Hazards and Environment, Chinese Academy of Sciences, Chengdu 610000, China
[b] University of Chinese Academy of Sciences, Beijing 100000, China
[c] China-Pakistan Joint Research Center on Earth Sciences, CAS-HEC, Chengdu, China
[d] National Research Council-Research Institute for Geo-Hydrological Protection (CNR-IRPI), Padova 35127, Italy

ARTICLE INFO

Keywords:
Debris flow
Dry avalanche
River blockage
Froude number

ABSTRACT

Debris flows are rapidly moving mixtures of water, rock, and soil that often occur in mountainous regions. When entering and depositing in river channels, they can obstruct the incoming water flow and generate secondary hazards such as outburst floods. Understanding the formation and failure of debris-flow dams is therefore critical for developing effective mitigation strategies and engineering countermeasures. This study investigates river blockage mechanisms through controlled flume experiments of debris flows with varying water contents. Further insights on the dam formation mechanisms are obtained from comparisons with recent findings on dry avalanches. The experiments show that the viscous pore fluid in debris flows reduces deflection upon entering the river, enabling them to form dams more readily than dry avalanches. Debris flow dams are generally thinner but extend across a wider section of the channel. These morphological differences also lead to contrasting outburst behaviors: dry-avalanche dams typically collapse abruptly under the impounded water load, whereas debris-flow dams are simply gradually eroded. The degree of blockage is governed by the relative dynamics of the debris flow and river flow. Based on this, we propose a predictive criterion using relative Froude numbers of the river and the debris flows that reliably distinguishes between blockage and no blockage in both experimental and real-world cases. These findings advance the understanding of river blockage processes and support more accurate hazard assessments in mountainous terrain.

1. Introduction

Debris flows are rapid geophysical mass movements consisting of a mixture of unsorted soil, rock fragments, organic matter, and water. Driven by gravity, they travel swiftly down steep hillslopes in mountainous terrain, posing serious threats to inhabitants and infrastructure downstream (Hutter et al., 1994; Iverson, 1997; Casagli et al., 2003; Takahashi, 2007; Chmiel et al., 2021; Kostynick et al., 2022; Cabral et al., 2023). When a tributary debris flow enters a river, the sudden influx of material may overwhelm the river's transport capacity. This imbalance leads to rapid deposition and damming of the incoming water flow. The increase of the impounded water may eventually lead to the collapse of the temporary dam resulting in catastrophic outburst floods (Swanson et al., 1985; Dang et al., 2009; Dong, 2011; Zou et al., 2020; Yu et al., 2022). Therefore, the convergence of debris flows into main rivers poses substantially greater risks than individual events (Chen et al., 2024c). One such event is the debris flow in the Hongchun Gully which dammed the Minjiang river on August 14, 2010. The dam failure resulted in the flooding of the town of Yingxiu, resulting in 13 deaths, 59 missing persons and 8000 evacuees (Dai et al., 2017; Shen et al., 2020). Given the severity of such events, it is therefore important to better understand the catastrophic consequences of debris flow-induced river blockage.

Insights into debris flow dam formation can first be gained from studies of dams created by dry avalanches, where pore fluid effects are negligible and flow dynamics are dominated by frictional and collisional

* Corresponding author at: Key Laboratory of Mountain Hazards and Engineering Resilience / Institute of Mountain Hazards and Environment, Chinese Academy of Sciences, Chengdu 610000, China.
E-mail address: gordon@imde.ac.cn (G.G.D. Zhou).

https://doi.org/10.1016/j.enggeo.2025.108422
Received 27 May 2025; Received in revised form 13 October 2025; Accepted 13 October 2025
Available online 14 October 2025

particle interactions. Our recent work on dry avalanches shows that the extent and geometry of river blockage by dry avalanches largely depend on the momentum of the incoming mass and the river's flow conditions (Luo et al., 2025). As the dry avalanche enters the river, the current can entrain and redistribute the material, altering the deposit pattern and the degree of blockage. Consider two avalanches of equal volume entering the same river: the one with lower velocity—and therefore lower momentum—is more easily dampened by the fluid drag as it enters the river and is readily diverted by the flow, often resulting in only partial blockage and continued water passage (Costa and Schuster, 1988; Liao et al., 2019; Nian et al., 2020). In contrast, a higher-momentum avalanche is more likely to overcome the retarding effect of fluid drag and is able traverse the full width of the channel. With its crest rising above the river's water surface, the dam forms a complete blockage that impounds significant volumes of water and increases the risk of catastrophic outburst flooding (Li et al., 2011; Tacconi Stefanelli et al., 2016; Luo et al., 2025). Similarly, a stronger river flow can overcome the momentum of a rapid avalanche, resulting in its deflection.

Debris-flow dams occur with a frequency comparable to landslide dams (Ruan et al., 2023). Similar to dry avalanches, the ability of debris flows to block rivers also depends on its interaction with the flowing river, particularly on their relative mobility (Chen et al., 2019a). However, unlike dry flows, debris flows are heavily influenced by their water content and degree of saturation (Hürlimann et al., 2015; Jakob et al., 2024; Kim et al., 2019). High pore pressures within saturated debris flows reduce frictional resistance and maintain fluidization, enhancing mobility and extending run-out distances (Takahashi, 2007; Chen et al., 2024a). These fluid effects not only increase the likelihood of river blockage but also affect the morphology and stability of the resulting dams (Chen et al., 2022; Cheng et al., 2024). Fluidized debris flows may form more extensive deposits that interact differently with the river flow, relative to that of dry avalanches, complicating predictions of dam persistence and failure. Yet, the complex interplay between saturation and downstream river response remains poorly understood. Advancing our understanding of these interactions is crucial for improving hazard assessments and managing debris flow risks in vulnerable mountain catchments.

Given the significant hazards posed by debris flow dams in mountainous regions (Stancanelli et al., 2014), research has increasingly focused on predictive strategies that can anticipate dam formation based on a limited set of known parameters (Chen et al., 2024). Experimental studies have attempted to identify threshold conditions for river blockage using dimensionless ratios such as the critical momentum ratio or discharge ratio, or through composite indices (Dang et al., 2009; Yu et al., 2022). However, these approaches rely on static thresholds and empirical parameters, overlooking the dynamic interplay between debris and river flows. Some researchers have proposed blockage criteria based on theoretically derived runout distances, deposition widths, and thicknesses (Du et al., 2014; Chen et al., 2019b) and but these methods also require extensive fitting parameters and do not capture the instantaneous dynamics of the process. Dynamics in the confluence zone tend to be more complicated (Chen et al., 2024). These modeling limitations can be overcome by considering the dynamic interactions between debris flow and river flow. In our recent work, we proposed a criterion for predicting complete and partial river blockages by dry avalanches based on the Froude numbers of both the avalanche and the river—dimensionless parameters that capture their flow dynamics. However, whether this approach extends to debris flow dams remains uncertain.

This study aims to investigate the formation processes and morphological characteristics of debris flow dams through flume experiments. Specifically, we study how interstitial fluid influences dam geometry and outburst hydrographs by comparing our results with those from dry avalanches (Luo et al., 2025). The following sections begin with a description of the experimental setup and materials. We then compare the experimental debris flows with real-world events using dimensionless analysis. The study proceeds to explore how debris flows interact with river currents, focusing on flow deflection, blockage morphology, and outburst behavior. From these findings, we identify distinct blockage states and propose an empirical criterion to predict complete versus partial damming based solely on the relative flow dynamics. Finally, we highlight key differences between debris flow and dry avalanche dams, emphasizing that early warning strategies developed for one may not be directly applicable to the other. This study reveals the mechanisms in which debris flows block rivers through direct observation of flow behaviors and by contrasting against the damming behaviors of dry avalanches. This work reveals that the dams formed by debris flows are less affected by the flow of the receiving rivers that they enter, resulting in thinner wider spanning dams. Through this knowledge, a Froude-number-based criterion for predicting debris flow blockages is proposed, which advances our understanding of how different types of mass movements obstruct rivers and provides a basis for forecasting river damming events.

2. Experimental method

2.1. Experimental apparatus and materials

The experiments were conducted at the Dongchuan Debris Flow Observation and Research Station (DDFORS), located in Dongchuan District, Kunming City, Yunnan Province, China (N26°14′, E103°08′). A schematic diagram of the experimental apparatus is presented in Fig. 1. A hopper with a maximum capacity of 0.08 m^3 releases debris flow material onto a·3 m flume whose bottom end intersects with another channel that serves as a modelled river. The flume is 0.4 m deep and 0.2 m wide and is inclined at a fixed angle of 20°, while the main channel is 5.1 m long, 0.4 m wide, and 0.4 m deep. Water flows through the main channel from an inlet that is 2.1 m away from the intersection of the two channels. An energy dissipation net is installed at the location shown in Fig. 1 to minimize turbulence of river flow. The base of the two channels is made of steel while the sidewalls are made of transparent glass which allows for the observation of the propagation and blockage processes. Four video cameras (SONY FDR AX40; 1440 × 1080-pixels, 25 fps) are used to investigate the propagation and deposition of debris flow and the movement of river flow. Additional details on the experimental set-up can be found in Luo et al. (2025).

All the test materials were collected from the debris flow fan of the Jiangjia Gully to simulate the wide grain-size distribution of the field materials (Fig. 2). The particles with diameters larger than 20 mm were removed using a 20 mm × 20 mm steel mesh in all tests (Zhou et al., 2019a, 2019b). Based on the debris flow grain-size distribution of materials in the Jiangjia Gully, grains with diameters less than 20 mm comprised 85 % of the total grain weight (Li et al., 2015). As this fraction dominates the rheological behavior of debris flows, the soil materials can be used to represent real debris flow materials (Wang et al., 2018). Fig. 2 shows that the Grain size distribution (GSD) of the debris flow materials used here are comparable to the range of distributions used in other debris flow experiments (Dang et al., 2009; Iverson et al., 2010; Zhou et al., 2019a, 2019b; Yu et al., 2022; Chen et al., 2024).

2.2. Testing procedures

In the experiments, rivers are simulated as continuous water flows in the main channel whose discharge is varied between 0.2 $L/s \sim 4.1$ L/s. The debris flows are simulated as mixtures of sun-dried soil and rock material collected from the Jiangjia Gully, with a constant mass of 50 kg, and variable amounts of water. The solid mass is held constant to ensure that there are equal amounts of material that can block the river in all cases. In doing so, increasing the volume fraction of water results in a slight increase of the total mixture volume, which may also affect the runout. To minimize these volume-related effects, water volume

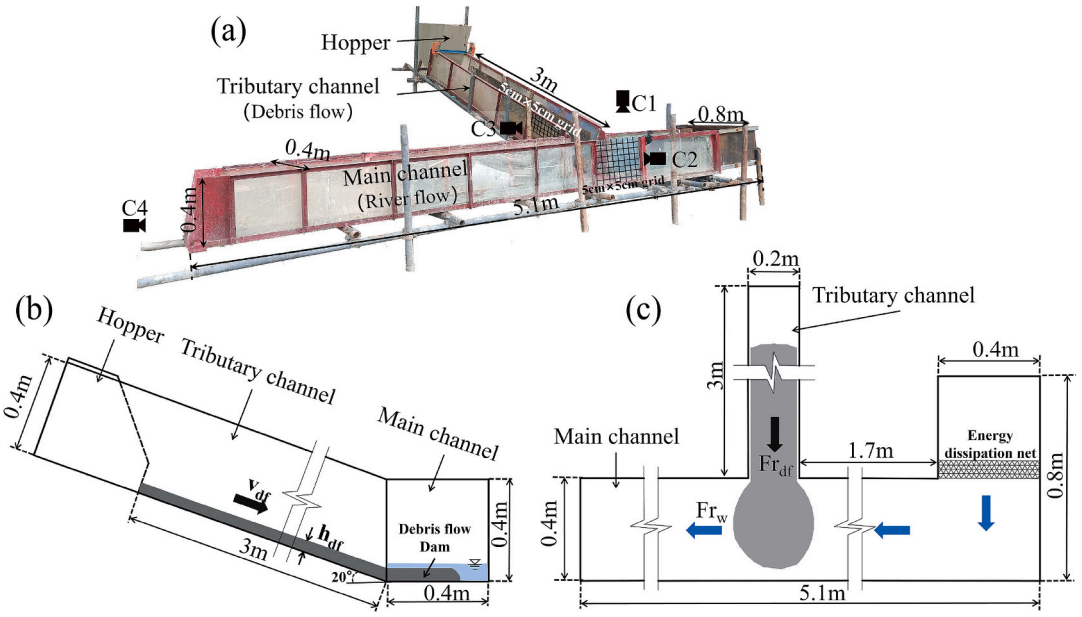

Fig. 1. Experimental apparatus used in the flume tests. (a) Snapshot of the experimental apparatus and locations of the measuring devices; (b) left side view and (c) top view of the apparatus.

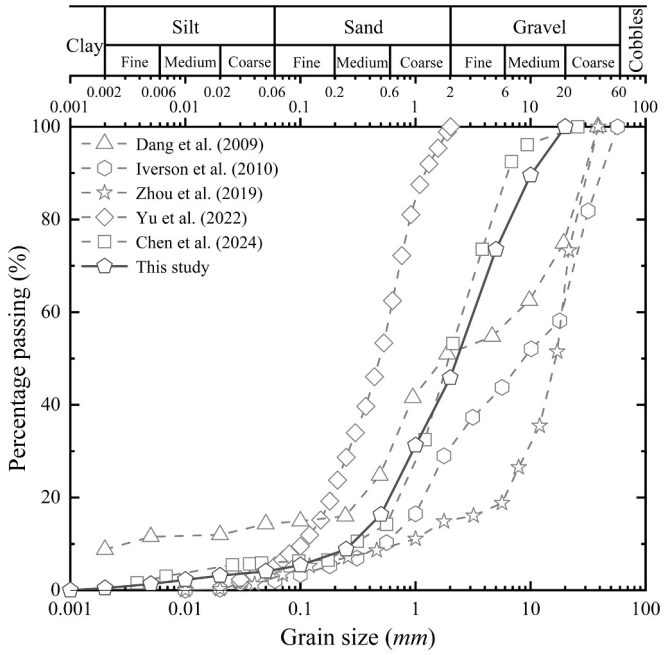

Fig. 2. Grain size distribution (GSD) curve of the debris flow material adopted in the experiments (the dark line). GSDs from other works are added for comparison.

fractions were only varied within a narrow range—20 %, 21 %, and 22 %—keeping the total mixture volume near 0.03 m^3. The water content of the experimental debris flow was determined to be within the range of the water content of the Jiangjia Gully debris flow (Jakob and Hungr, 2005). Despite this minimal change in the levels of saturation, its impacts on the mobility are clearly observable, as discussed in the Results section. Debris flow materials were precisely weighed, homogenized by electric mixing for 10 min, and re-weighed before loading to ensure consistent mass and composition. The experiments consist of 18 tests designated into six groups (labelled A-F) where each group is characterized by the river flow discharge. In each group, the debris flow water content is varied. Details of all tests are summarized in Table 1. Group A serves as the control set-up where the debris flow enters onto a dry bed.

Once the river flow was stabilized, the debris flow material was released to move freely along the tributary channel by opening the gate in the front of the hopper. The layout of the cameras is shown in Fig. 1. Camera 1 (C1), positioned above the intersection of the two channels, recorded the interaction of the debris flow and river flow, and the deposition process. Camera 2 (C2), installed perpendicular to the main channel to view through a grid (5 $cm \times$ 5 cm), was used to record the intrusion of the debris flow and observe the river flow movement. Camera 3 (C3) located on the left side downstream of the tributary channel was used to record the process of debris flow movement. Camera 4 (C4) was placed at the downstream end of the main channel to record the movement of debris flows in the river. Foam balls, 5 $cm \times$ 5 cm grids and rulers on the side wall were used to obtain the velocities and flow depths of the debris flows and the river flows (before and after the formation of debris flow dams) by extracting and analyzing video data frame by frame.

The dynamics of both the debris flows and river flows are characterized by the Froude number (Fr) which is the ratio of the inertial to gravitational forces:

$$Fr = \frac{v}{\sqrt{gh\cos\theta}} \tag{1}$$

where v and h are the velocities and depths, θ is the slope angle, g is gravitational acceleration (9.8 m/s^2). For clarity, quantities for debris flows are assigned a subscript df while w is used for quantities of water. The Froude number of dry avalanches, obtained from Luo et al. (2025), which are used to contrast with our results are represented by a subscript. Since the river channel is horizontal, the $\cos\theta$ term is unity: $Fr = \frac{v}{\sqrt{gh}}$, reflecting the wave-making resistance in free-surface flow (Choi et al., 2015b; Yan et al., 2023). The Froude number is used since it relies on easily measurable parameters and it is already widely applied to characterize both debris flows and rivers in the literature (Liu et al., 2024). The Fr_w and Fr_{df} values of each test set up, including the relevant parameters used to calculate them are summarized in Table 1.

To better appreciate the effect of fluid content on the mobility of the simulated debris flows, their motion is further characterized by dimensionless quantities that quantify the relative importance of iner-

Table 1
Summary of debris flow and river flow related parameters characterizing each test.

Group ID	Tests	Q_w (L/s)	W (%)	h_w ($\times 10^{-3}\ m$)	v_w (m/s)	h_{df} ($\times 10^{-2}\ m$)	v_{df} (m/s)	Fr_w	Fr_{df}	River blockage mode
	A-1		20	–	–	2.2	0.030	0	0.067	–
A	A-2	0	21	–	–	3.8	1.745	0	2.950	–
	A-3		22	–	–	3.4	1.983	0	3.544	–
	B-1		20	3.2	0.143	2.8	0.040	0.808	0.079	NB
B	B-2	0. 20	21	3.0	0.136	4.0	1.735	0.793	2.859	B
	B-3		22	3.2	0.136	2.8	2.200	0.768	4.332	B
	C-1		20	7.5	0.345	3.0	0.037	1.273	0.070	NB
C	C-2	0. 90	21	6.8	0.323	3.8	1.855	1.251	3.136	B
	C-3		22	7.5	0.333	3.4	1.925	1.228	3.440	B
	D-1		20	12.0	0.457	2.8	0.030	1.333	0.059	NB
D	D-2	2. 10	21	12.0	0.444	3.3	1.798	1.295	3.262	B
	D-3		22	12.0	0.444	2.8	1.925	1.295	3.790	B
	E-1		20	14.3	0.625	2.8	0.032	1.670	0.063	NB
E	E-2	3. 60	21	14.1	0.588	3.6	1.684	1.582	2.925	NB
	E-3		22	15.0	0.625	3.0	1.937	1.630	3.685	NB
	F-1		20	16.6	0.589	2.8	0.031	1.460	0.061	NB
F	F-2	4. 10	21	15.7	0.564	3.4	1.680	1.438	3.002	NB
	F-3		22	16.5	0.585	3.0	1.820	1.455	3.463	NB

Note: B represents 'blockage' while NB indicates "no blockage".

tial, frictional, and viscous forces on the material transport (Iverson, 1997; Stancanelli et al., 2015; de Haas et al., 2015; Zhou et al., 2019a, 2019b). The ratio of grain-inertial-to-contact frictional forces is defined as the Savage number:

$$N_{sav} = \frac{\rho_s \delta^2 \dot{\gamma}^2}{(\rho_s - \rho_f) g h_{df} tan\varphi} \tag{2}$$

Bagnold number N_{Bag} is quantified as the ratio of inertial to viscous forces:

$$N_{Bag} = \frac{V_s \rho_s \delta^2 \dot{\gamma}}{(1 - V_s)\mu} \tag{3}$$

where the interstitial fluid viscosity μ is calculated considering the volume fraction of the suspended fine particles (Iverson, 1997):

$$\mu \Big/ \mu_w = 1 + 2.5 V_{fines} + 10.05 V_{fines}^2 + 0.00273 e^{16.6 V_{fines}} \tag{4}$$

where μ_w is the dynamic viscosity of pure water (0.001002 $Pa \bullet s$), and V_{fines} is the volume fraction of fine particles less than 2 mm (Cui et al., 2015; Chen et al., 2023),. Friction number N_{Fric} is defined as the ratio of grain-contact to fluid viscous forces:

$$N_{Fric} = \frac{V_s (\rho_s - \rho_f) g h_{df} tan\varphi}{(1 - V_s)\dot{\gamma}\mu} \tag{5}$$

where δ is the mean grain size of the solid particle, V_s is the volumetric solids fraction of particles with more than 2mm, $\dot{\gamma} = \frac{v}{h_{df}}$ is the flow shear rate (s^{-1}), v is flow velocity (m/s), h_{df} is flow depth (m), g is gravitational acceleration (9.8 m/s^2), φ is the internal frictional angle which is 30° for the debris flow materials in the Jianjia Gully (Zhou and Ng, 2010; Zhou et al., 2019a, 2019b), ρ_s the solid particle density (2650 kg/m^3, Chen et al. (2023)), ρ_f is the fluid density and $\rho_f = \rho_s V_{fines} + \rho_w (1 - V_{fines})$, where $\rho_w = 1000\ kg/m^3$ is the density of water.

3. Results

3.1. Dimensionless characterization of the experimental debris flows

Fig. 3 shows the range of Froude numbers of the experimental debris flows plotted against their N_{Bag}, N_{Sav}, and N_{Fric} values. To better highlight the effects of the interstitial fluids on the mobility, the debris flow data is compared with data from dry avalanches obtained from Luo et al. (2025). To improve the relevance of this work, the dimensionless quantities of the experimental debris flows are compared with those of de Haas et al. (2015) and real debris flow data in the literature (see Table 2 in Appendix), specifically those that resulted in river blockage (see analysis in Section 3.4). The debris flow experiments of de Haas et al. (2015) provide a good comparison for our tests since they are conducted in a similar scale, although they used a wider range of water content and a broader GSD. According to Choi et al. (2015a), the Froude number of debris flows in the field ranges from 0.5 to 7.6. while the documented range for the N_{Bag}, N_{Sav}, and N_{Fric} of real and experimental debris flows are $1 \sim 10^8$, $10^{-7} \sim 1$, $1 \sim 10^5$ (Iverson, 1997; Iverson and Denlinger, 2001; Zhou and Ng, 2010), respectively. These ranges are indicated by gray bands in Fig. 3. Critical dimensionless thresholds of N_{Bag}, N_{Sav}, and N_{Fric} serve as benchmarks that characterize the dominant driving mechanisms behind debris flow behavior (Iverson, 1997). Thresholds established in previous studies suggest that collisional forces dominate over viscous forces when $N_{Bag} > 200$, frictional forces dominate over viscous forces when $N_{Fric} > 2000$, and collisional forces dominate over frictional forces when $N_{Sav} > 0.1$ (Iverson, 1997; de Haas et al., 2015; Zhou et al., 2019a, 2019b).

The Froude numbers of the experimental debris flows (Fr_{df}) range from 0.05 to 4. The cases having 20 % water content are much lower than those with 21 % and 22 % water content and even fall below $Fr_{df} < 0.5$. The slight increase in water content result in flows that fall within the limits corresponding to real debris flows. This shows that the small changes in the water content used in this work result in dramatic changes in the debris flow mobility. Except for low water content groups (20 % water content) that show low N_{Bag} values, very high N_{Fric} values and low N_{sav} values, most experimental debris flows are mainly controlled by collisional interactions (Fig. 3a and Fig. 3b). Despite the presence of muddy interstitial fluids, frictional forces still dominate over viscous ones, as shown in Fig. 3c.

Data for dry avalanches are very distinct from those of the debris flows. The Froude numbers (Fr_s) of the dry avalanches on the other hand range from 5 to 7. The N_{Bag}, N_{Sav} and N_{Fric} of all dry avalanches are high, and far exceed that of the debris flows showing that with the negligible influence of the interstitial fluid, their transport is primarily governed by grain collisional forces (Zhou et al., 2020). The difference in the mobility of the two flow types results in distinct interactions with the river, leading to different deposit morphologies and outburst mechanisms, as will be detailed in subsequent sections.

The N_{Bag} and N_{Sav} values of the natural debris flow closely correspond to those of the experiments and span over the same range of Fr_{df}. The N_{Fric} for the natural cases are slightly larger possibly due to the

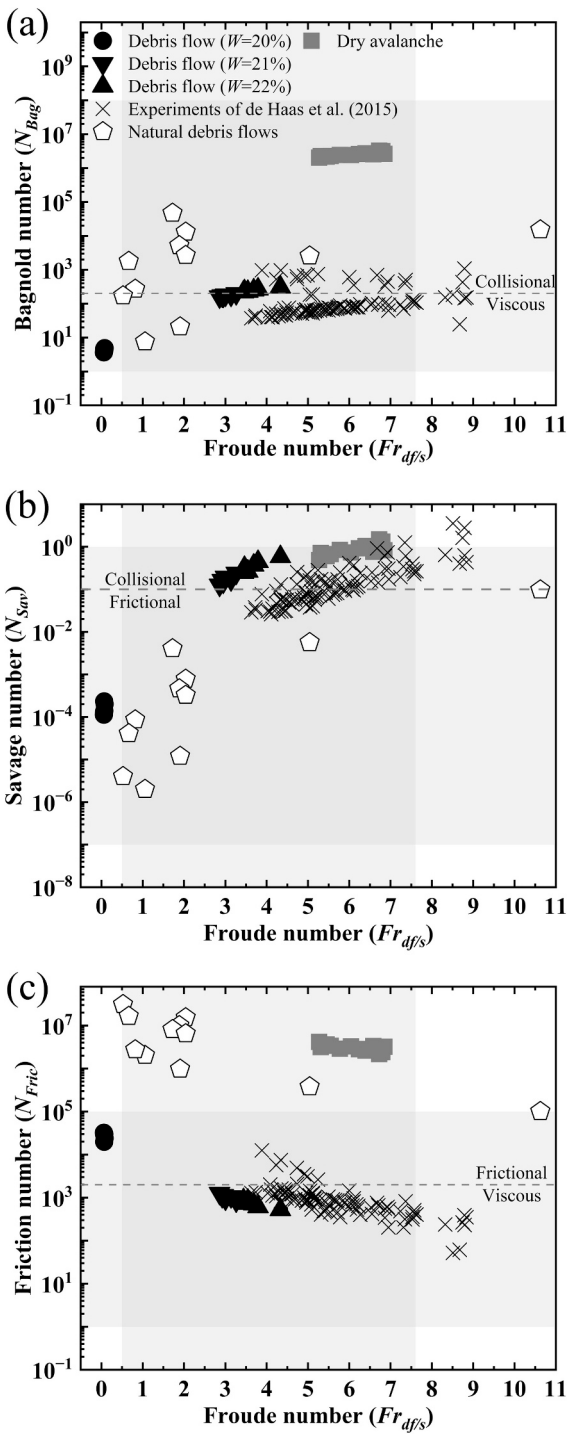

Fig. 3. Dimensionless characterization of the experimental debris flows using the (a) Bagnold number N_{Bag}, (b) Savage number N_{Sav}, and (c) Friction number N_{Fric} plotted against their Froude number Fr_{df}. Debris flow data is compared with those of dry avalanches obtained from Luo et al. (2025) whose flow is characterized by Fr_s. Gray bands represent the documented range of these dimensionless constants. Dashed lines are boundaries that represent the transition between dominant transport mechanisms (Iverson, 1997). The Field cases and data from de Haas et al. (2015) are also used for comparison.

reduced influence of slurry viscosity in more massive flows, although they still scale closer to the experimental debris flow compared to the dry avalanche data. We further compare our experimental debris flows with those of (de Haas et al., 2015), who mainly investigated effects of debris flow composition on runout, depositional mechanisms, and deposit morphology. It is observed that their experiments have slightly lower N_{Bag} and N_{Sav}, while their N_{Fric} scales well with our data. Which is probably to the lower thicknesses of their flows ($0.005m \sim 0.018m$ while they are $0.022m \sim 0.04m$ in our study) resulting in higher shear rates. Despite the discrepancy, our experimental data exhibits the same scaling behaviors with the data of de Haas et al. (2015) and with the natural cases in the parameter space considered. These observations show that the experimental debris flows presented here are dynamically comparable to natural events and other debris flow experiments and may reasonably replicate the mechanisms through which debris flows block rivers.

3.2. Debris flow intrusion process

When a debris flow is released from the flume and enters the downstream river channel, it interacts dynamically with the flowing water. Fig. 4 illustrates a representative example of a debris flow entering the river channel, based on test F-2. The debris flow first reaches the end of its flow channel and makes contact with the downstream river (Fig. 4a). Except for the cases with 20 % water content which barely reach the base of the inclined flume, the debris flows normally plough through the river to reach the opposite bank (Fig. 4b). As it moves through the water, it is deflected along the direction of the river, spanning over a portion of the river channel in the upstream and downstream directions. At the intersection of the river and inclined flume the deposit is thickest and significantly obstruct the river flow (Fig. 4c). In the example case F-2 the dam is mostly submerged, but in some cases the dam height is greater than that of the river. Continuous river flow either destroys the dam or erodes it (see Section 3.3 for details), transporting the finer particles downstream, leaving the coarser grains to form the dam. Some of the fine particles also become immediately suspended upon entry into the river (Fig. 4c) and get immediately washed away. At the end of the experiment, which is when the dammed river flow is clear of suspended sediment and a terminal dam structure is evident, the inflowing water is turned off revealing the final dam profile (Fig. 4d). As indicated in Fig. 4, L_1 and L_2 represent the lengths from the dam upstream and downstream to the central line of the tributary channel, respectively. The widths of the tributary and main channels are 20 cm and 40 cm.

The extent in which the debris flow is deflected by the river depends on the relative momentum of the two flows (Nian et al., 2020; Luo et al., 2025). Both the debris flow and the river are characterized by the Froude number and their interaction can be quantified by the ratio between them:

$$Fr^* = Fr_{df}/Fr_w \tag{6}$$

If the Froude number ratio Fr^* is greater than 1, the debris flow is more mobile than the river flow; if $Fr^*<1$, the river flow moves faster. When the $Fr^* \sim 1$, the debris flow has comparable mobility to the river.

The extent in which the river influences the debris flow trajectory can be measured from the degree of its deflection. We measure deflection in two directions as the longest distance the debris flow has travelled, from centerline of the tributary channel, upstream L_1 (against the river flow) and downstream L_2 (along the river flow) (see Fig. 4). Information on the preferred direction of deflection can be gained from the ratio of the two distances:

$$L^* = L_2/L_1 \tag{7}$$

where $L^* > 1$ indicates that the debris flow primarily spreads in the direction of river flow, $L^* < 1$ implies spreading against the flow, while $L^* = 1$ means the solid material is spreading equally in both directions. These distances are measured from the photographic data when the debris flow first reaches the opposite flume wall (Fig. 4b), and at the end of the experiment, after the water pump has been turned off (Fig. 4d).

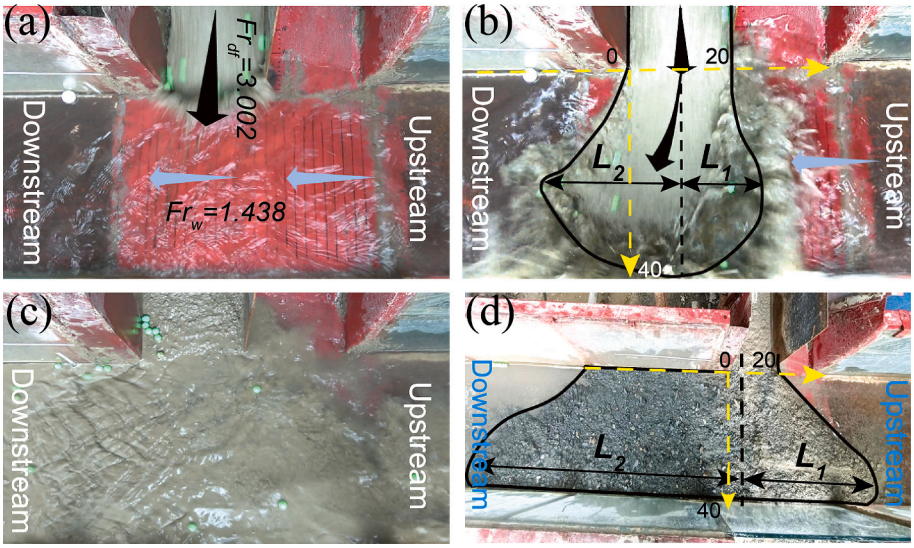

Fig. 4. A typical debris flow dam formation process of an example test F-2. (a) The debris flow enters the river, and (b) reaches the opposite bank. (c) The debris flow deposits in the river and forms a dam. (d) The final debris flow dam profile after the river flow is terminated. L_1 and L_2 are the upstream and downstream dam lengths from the tributary channel centerline, respectively. Channel widths are 20 cm (tributary) and 40cm (main).

For convenience, we refer to the two different measurement times in the deflection process as Stage 1 and Stage 2 respectively. Measuring at these two stages enables the evaluation of the effects of immediate and prolonged interaction between the debris flow dam and flowing water. Tests with 20 %, water content are exempted from this analysis since in these cases the debris flow does not reach the opposite bank. The L_1 and L_2 measurements for dry avalanches (Luo et al., 2025) are also shown here for comparison.

Fig. 5a and b show the change of L_1' and L_2', for both debris flows and dry avalanches, with the Fr^* respectively. Here, $L_1' = L_1/b$ and $L_2' = L_2/b$ are dimensionless distances (b is the width of the tributary channel and $b = 0.2$m for both debris flow and dry avalanche). Measurements at Stage 1 are represented by the filled symbols while those at Stage 2 are unfilled. At Stage 1, the deflection in both upstream and downstream directions are minimal. In this initial and transient stage, the solid material of both the debris flows and the dry avalanches spread over the same distance (~1) regardless of Fr^*. This shows that the solid mass, either fluid-laden or dry, is not significantly re-directed upon entering the river. On the other hand, the data in Stage 2 are much greater than in Stage 1 since the solid mass of both debris flows and dry avalanches have been exposed to the continuous water flow and, in some cases, have been spread by the outburst flood (see Section 3.3). Comparing the data in Stage 1 and Stage 2, the change in the spread of material is much more evident for the debris flows than it is for the dry avalanche. Interestingly, the L_1' for the debris flows are comparable to their L_2' (both ~4.5), while the distinction is clear for the dry avalanches wherein, on average, L_1' is an order of b less than L_2'. The extensive spread of the debris flow material suggests that their deflection is unaffected by the river flow. To investigate this, we plot in Fig. 5a and b the mean L_1' and L_2' of debris flow experiments without river flow, where the spread of the material is only because of the debris flow's impact against the opposite wall. The L_1' of debris flows with $Fr^* \lesssim 3$ is slightly shorter, while the L_2' is slightly greater than in the absence of a river, indicating that the river flow still exerts a minor influence on deposit geometry. For faster-moving debris flows, however, the spreading pattern remains largely unaffected by the river, as evidenced by the similarity to cases without river flow. Fig. 5c shows that for both flow types the L^* exponentially decreases with Fr^* showing that when the mass flow has significantly greater momentum than the river, it tends to spread out evenly. The L^* for dry avalanches, are much greater than that of the debris flows revealing that dry avalanches undergo greater deflection under equivalent hydrodynamic conditions. The weak dependence of the debris flow deflection on the river flow is further evidenced by their L^* values which are all close to 1 specially when the flow has relatively higher mobility.

Although the limited deflection of the debris flows is somewhat surprising—given that more fluid flows are typically more susceptible to redirection-it can be explained through the cohesive nature of the fine-grained slurry. The slurry binds solid particles together, enabling the mass to move as a more coherent, viscoplastic block that can traverse the channel with minimal lateral spreading. Furthermore, the low permeability of this saturated matrix prevents the internal pore fluid from escaping and simultaneously inhibits the ingress of river water into the flow body. This dual action enhances internal fluidization and mobility—while also drastically reduces the transmission of hydrodynamic drag forces from the river that would otherwise promote deflection and entrainment of individual particles. Both the Savage number N_{Sav} and Friction number N_{Fric} (Fig. 3) indicate that, although the experimental debris flows are collision-dominated, the influence of viscous forces in the material transport is more relevant than in the dry avalanches. The N_{Fric} for debris flows decreases with their Froude number Fr_{df}, further indicating the growing influence of slurry viscosity. This trend coincides with reduced deflection, suggesting that viscous effects helps maintain a more compact flow structure (Zhang and Cui, 2013). In addition, viscous damping suppresses particle fluctuations and dispersion (Cui et al., 2021), reducing their likelihood of being carried away by the river. Together, these effects make debris flows more resistant to deflection by ambient water flow.

3.3. Degrees of blockage and resulting dammed-water hydrographs

The blockage scenarios observed in our experiments, categorized as either 'No blockage' (NB) or 'Blockage' (B). A case is classified as NB when the debris flow only partially obstructs the river—allowing water to flow along the edges or when the dam is submerged and water flows over it. Blockage occurs when the dam height exceeds that of the river, temporarily obstructing the water flow. Based on this classification, the results of river blockage in the experiments are shown in Table 1.

The formation of a debris-flow dam raises the upstream water level. Fig. 6 presents the corresponding dammed-water hydrographs for blocked (Fig. 6a) and unblocked (Fig. 6b) cases, expressed in terms of the dimensionless water depth ratio h_t/h_w and dimensionless time t^*.

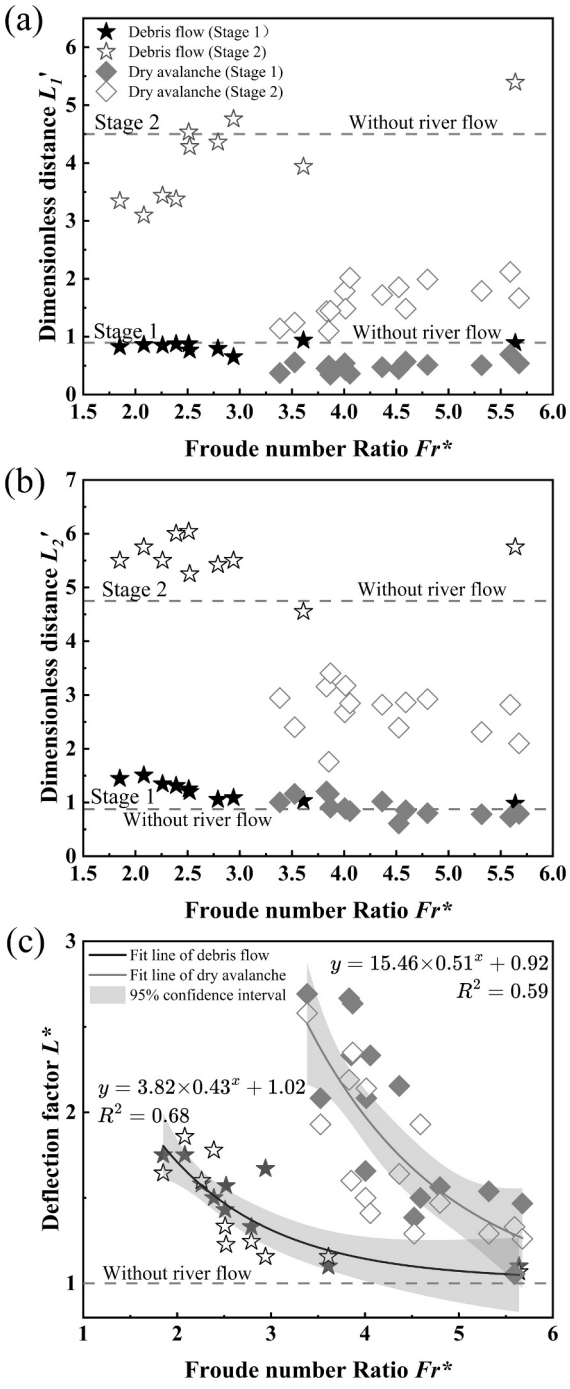

Fig. 5. The change of (a) Upstream distance, L_1' (b) downstream distance, L_2', and (c) deflection factor, L^* with relative Froude number, Fr^*. Filled markers represent the first stage (Stage 1), hollow markers represent the second stage (Stage 2). Solid lines are best-fits of the exponential functions written within the plots. The dark line is the best fitting line for debris flow, while the light-colored line is for dry avalanche. The shaded areas represent the 95 % confidence intervals.

Here, $t^* = t/\sqrt{h_w/g}$, where t is the actual time during the experiment, h_w is the initial river flow depth, and h_t is the flow depth at time t. The values of h_t and h_w are obtained by frame-by-frame analysis of videos recorded by Camera 1 and Camera 2. The hydrographs for both blockage scenarios can be divided into three stages: initial, rising, and stable. The initial stage begins when the debris flow makes contact with the water surface until the moment when the water level starts to change. The

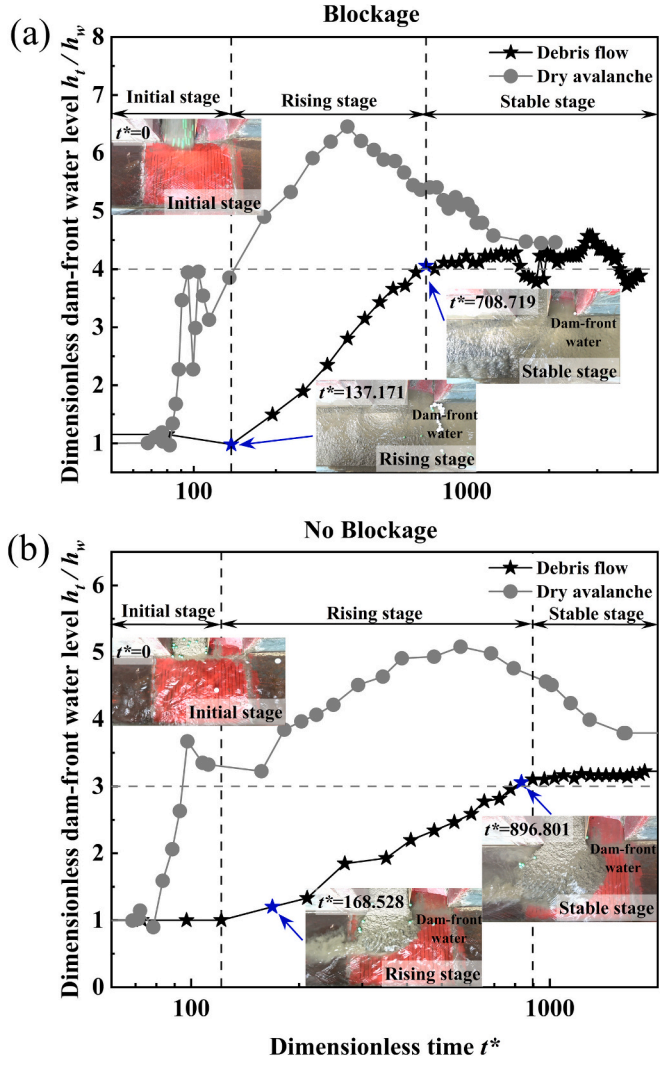

Fig. 6. The variations of dimensionless dam-front water level h_t/h_w with dimensionless time $t^* = t/\sqrt{h_w/g}$ for a (a)blockage case (B) and a (b) no blockage case (NB). The black solid pentagram point and the gray solid circle point represent B mode of debris flow and dry avalanche, while the black hollow pentagram and the gray hollow circle represent NB mode of debris flow and dry avalanche. Snapshots of the different stages obtained by camera 1 (C1) are also placed in the figure.

rising stage is defined as the period from the beginning of the water-level increase in front of the debris-flow dam until stabilization is reached. The stable stage begins when the water level fluctuations can be ignored. We selected screenshots near the critical event nodes during various stages after the debris flow entered the river, and placed them in the diagrams. In addition, we compared the variation of dam-front water level between debris flows and dry avalanches in two different river blockage modes to investigate the similarities and differences. The selected tests (C-2; F-1) and corresponding dry avalanche tests have similar Froude numbers of river flows.

Fig. 6a shows that at the rising stage (t^* = 137–708) of a completely dammed river, the dam-front water level steadily rises due to the constant inflow rate. This phase is characterized by a predictable and steady rise in water level, which is a critical aspect for understanding the rising stage of dam formation and its impact on upstream water levels. During the process of the water level rising in front of the dam, the outflow of water downstream of the dam is zero, and the water level in front of the dam continues to rise. At t^*~700, the hydrograph reaches the steady stage where h_t/h_w stabilizes into a constant value of ~4. The small

fluctuations are due to the river's weak yet constant scouring of the dam surface. This means that the dam did not abruptly collapse, raising the elevation from which the river flows. Fig. 6b shows that for a partially blocked river, the hydrograph largely follows a similar process to that of the completely blocked case, except that for a partially blocked river the Rising stage is much longer (ending at $t^* = 896$) and the terminal height in the Stable stage is lower ($h_t/h_w \sim 3$).

The upstream hydrographs of debris flow dams are noticeably different from those of dry avalanches. Dams formed by the dry avalanches are thicker and impound greater amounts of water which are then eventually rapidly released upon the collapse of the dam. This is reflected in the high impounded water levels which rapidly decrease towards a constant value that is higher than h_w. The difference in the dammed water hydrographs exhibit different breaching dynamics between dams formed by dry avalanches and debris flows. While dams from dry avalanches collapse to release outburst floods, debris flows dams are slowly eroded away. This difference in outburst flooding behaviors is likely related to the initial dam height formed by the two types of flows. Debris flow dams are generally lower than the dry avalanche dams and impound a lower water height which exert lower pressures on the dam (Chen et al., 2024c). While dry avalanches are cohesionless, debris flow materials are held together by cohesive slurry creating a stronger dam body.

3.4. Froude number-based criterion for determining river blockage by debris flow

Predictive models for river blockage are critical for early risk identification and disaster prevention, enabling timely mitigation of catastrophic dam breaches and downstream flooding (Dang et al., 2009; Chen et al., 2019a; Zeng et al., 2024). Since the relative Froude numbers determine the shape of the deposits, it may also be used to predict the cases when a debris flow can block a river based on its relative motion with the river. In Fig. 7, we plot our data in the Fr_{df}-Fr_w phase space wherein the B cases are represented by filled symbols while hollow symbols are used for the NB cases. Experimental data from the two blockage scenarios form distinct clusters in the phase space. To separate

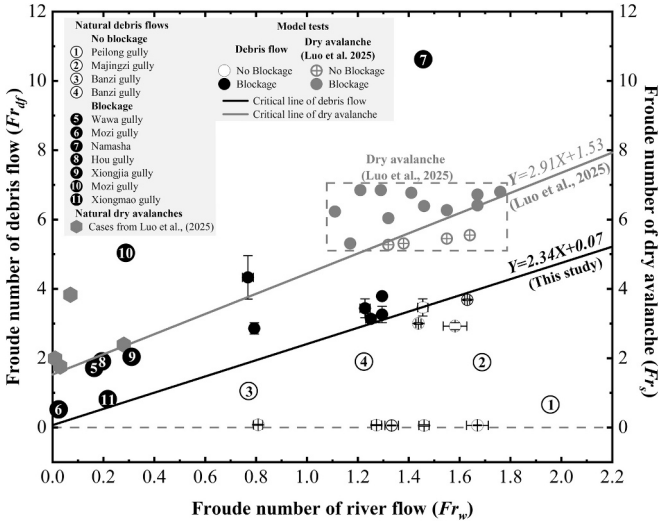

Fig. 7. The experimental data plotted according to their Fr_{df} and Fr_w. Filled symbols represent "blockage" cases, while hollow symbols indicate "no blockage." Numbered markers, following this fill convention, correspond to real-world debris flow dam events. Gray circles denote dry avalanche experiments from Luo et al. (2025), and gray decagons represent actual landslide dam cases summarized in the same study. The lines indicate classification boundaries that separate the 'blockage' and 'no blockage' cases. The lighted-colored line above is critical lines for dry avalanche, while the other black line is for debris flow.

these clusters, we apply a simple single-layer perceptron algorithm, resulting in a linear decision boundary of the form:

$$Fr_{df} - AFr_w - B = 0 \tag{8}$$

where A and B are fitting parameters. While the data separation is visually apparent and could be divided by an arbitrary linear boundary, we adopted a more data-driven approach using a simple machine learning algorithm. Data points above the critical line correspond to river blockage, whereas those below it do not reach the threshold required to induce dam formation. When Fr_w is held constant, Fr_{df} emerges as a key indicator of blockage potential. As Fr_w increases, a proportionally higher Fr_{df} is needed to block the river, reflecting the dynamic interplay between the debris flow and river flow regimes.

A similar classification strategy was used in our previous work to assess river blockage by dry avalanches, resulting in a linear boundary with a similar form to Eq. 8. Fig. 7 shows the data points from Luo et al. (2025), along with the classification line for the dry avalanches. The critical line for debris flows is defined by parameters $A_{df} = 2.34$, $B_{df} = 0.07$, while dry avalanches have $A_s = 2.91$, $B_s = 1.53$. The differing slopes and intercepts of the two critical lines reveal important distinctions in blockage behavior. The slope represents the increase in debris or avalanche Froude number (Fr_{df} or Fr_s) required to overcome a unit increase in river Froude number (Fr_w) and still achieve blockage. The steeper slope of the dry avalanche line suggests that its ability to block the river is less sensitive to changes in river flow and requires a greater increase in its own momentum to offset the scouring effect of the water. This is consistent with its greater susceptibility to deflection. The y-intercept of each line represents the critical Froude number required for blockage when there is no river flow. The higher intercept for dry avalanches (B) indicates that, even in the absence of river flow, a higher kinetic energy is still needed for blockage compared to debris flows. In contrast, the lower intercept of the debris flow line suggests that debris flows can block rivers even under relatively low flow conditions. The non-zero intercept of 0.07 holds significant physical meaning, representing the minimum Froude number required for a debris flow to cause blockage. This threshold indicates that even if the mainstream flow is hydrostatic, the debris flow still needs sufficient momentum to overcome the resistance of the river flow and form a stable debris flow dam.

To validate the predictive capabilities of the critical line, the data for the 11 debris flow events featured in Fig. 4 are cast onto the Fr_{df}-Fr_w space in Fig. 7. Of the collected cases, 7 are classified to have resulted in river blockage (based on the criteria applied on the experimental debris flow dams), while 4 result in no blockage. These classifications are consistent with field observations, where the same seven cases indeed resulted in river blockage. This agreement provides encouraging insights that may contribute to hazard assessment and the development of preventive strategies.

This distinction is further supported by comparing the debris flow from Table 2 and real dry avalanche (i.e., landslides) cases collected by Luo et al. (2025). Debris flows exhibit a broader Froude number range ($0.522 \sim 10.624$) compared to landslides ($1.76 \sim 3.83$). The corresponding river Froude numbers are also higher for debris flow cases ($0.024 \sim 1.957$) than for landslides ($0.01 \sim 0.28$). Notably, five out of the seven B-mode debris flow events occurred at $Fr_{df} < 2$, with one case as low as 0.522. Blockage was still observed even when the river Froude number reached 1.457. In contrast, dry avalanches required higher slide Froude numbers and occurred in settings with relatively low river flow. These comparisons underscore that, under similar river conditions, debris flows are more likely to induce blockage than granular landslides. This supports the conclusion that debris flows pose a higher blockage risk and are more responsive to dynamic river interactions.

4. Discussion

This study systematically investigates the complete process of river

blockage by debris flows through a series of controlled flume experiments, aiming to develop a predictive criterion for distinguishing different blockage modes. To highlight the unique characteristics of debris flows, results are compared with recent findings on dry avalanches. A conceptual model (Fig. 8) is proposed to summarize the interaction between both flow types and river flows, along with the criteria for classifying blockage behavior.

The processes of debris-flow dam formation, outburst flooding, and their differences from dry avalanches are summarized conceptually in Fig. 8. Upon entering the river, debris flows with ~20–22 % water content (our experimental configuration) generally spread easily on the river channel with little interference from the river flow, i.e., the debris flow moves both along and against the river's direction. We attribute this enhanced runout to the effects of the viscous pore fluid, which either promotes cohesive forces between particles (Zhou et al., 2019a, 2019b) or acts as a dense matrix that prevents river water from penetrating the flow body and dragging particles downstream (see Fig. 5). The slurry may also inhibit excess fluid from escaping, thereby contributing to further fluidization (Iverson, 1997). Depending on the relative dynamics of the debris flow (controlled by water content) and the river flow, the river may be completely blocked (Fig. 8b), where the material reaches the opposite bank, or only partially blocked (Fig. 8c). Because debris-flow material spreads more widely, the resulting dams are relatively thin. In blockage scenarios (Fig. 8b), the impounded water volume remains small, and erosion is limited to the dam surface, producing no abrupt changes in the flood hydrograph. In contrast, in partial blockage cases (Fig. 8c), the river flow primarily erodes the dam's outer edges.

In contrast to the debris flow damming process, the trajectory of dry avalanches in the river is more easily re-directed by the river flow (Fig. 8d) but more easily deposits at the foot of the channel possibly since the material transport is dominated by frictional-collisional interactions among particles. The dam is thicker and steeper at the faces and, in a blockage scenario, would impound a large volume of water. When the impounded water begins to overtop the dam, it carves a narrow path or notch on the dam surface (Fig. 8e) (Zhou et al., 2019a, 2019b), which will eventually develop into a large-scale collapse. If the blockage is only partial (Fig. 8f), as with the debris flow dams, the river will simply erode the edge of the deposits.

The difference in the interaction of debris flows and dry avalanches with the downstream river results in different probabilities of blockage. Debris flows do not need to be as mobile as dry avalanches to block a river. In our Froude number based predictive criteria in Fig. 7, the contrast in blockage probability is manifested as an upward shift in the classification curve. In order to mitigate the outburst flooding risks, it is advantageous to rapidly assess the probability and geometry of landslide or debris flow dams. The results in this work show that the predictive criteria for river blockage by geophysical flows in mountainous areas, should be distinct depending on the presence of pore fluid.

The results demonstrate that the flow dynamics of both the debris flow and the river flow are critical factors affecting the formation of blockage dams. The flow dynamics and discharge do not correspond uniquely, so the flow discharge cannot reflect the flow dynamics well (Luo et al., 2025). Therefore, Froude number, instead of discharge, is used to characterize flow regimes in this study. The Froude number of debris flows can be estimated through field investigations, while the Froude number of rivers can be obtained from local hydrological stations. By substituting the obtained values into the equations, we can determine the likelihood of disasters occurring due to river blockage.

In this research, it is assumed that the width of the river and the volume of debris flow are constant. However, the river width and debris flow volume are also decisive factors for debris flow inducing river blockage (Du et al., 2014; Braun et al., 2018; Zeng et al., 2024). If there is a large river with a wide channel, the debris flow continues to interact with the river flow during its movement to the opposite bank. Some

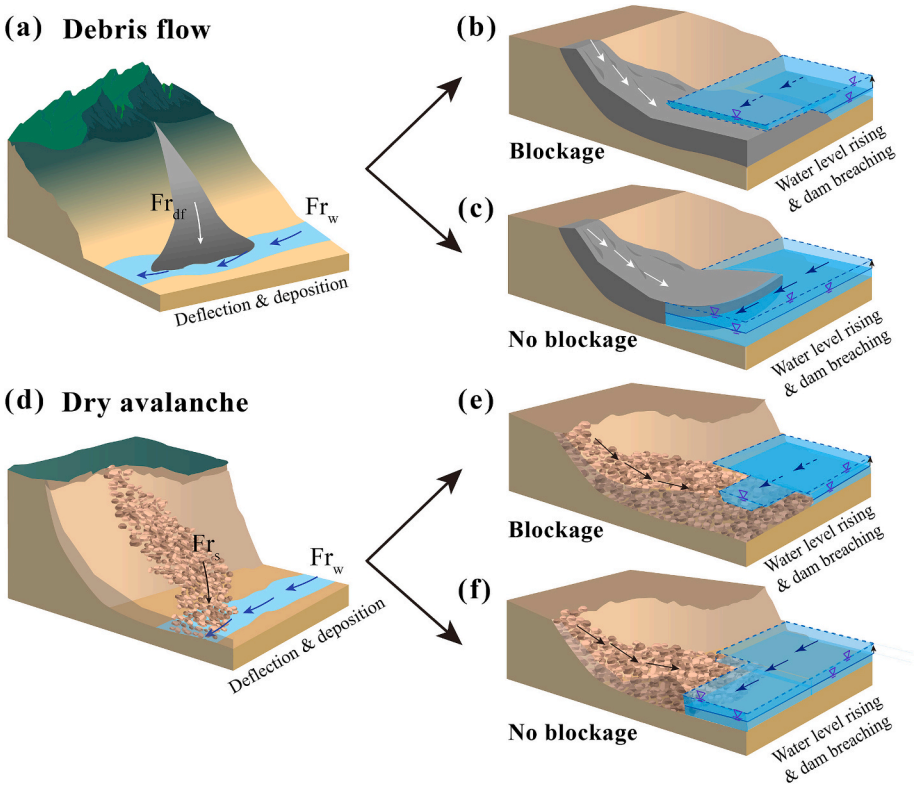

Fig. 8. Summary of river blockage processes by debris flows and dry avalanches. (a) Debris flows entering the main river with minimal deflection. (b) Overtopping flood eroding the debris flow dam crest in a blockage scenario and (c) erosion by the river flow at the dam boundaries in a no blockage scenario. (d) Dry avalanches entering the river, showing significant re-direction. (e) A blockage scenario where the overtopping usually occurs at a notch at the dam crest, (f) whereas in a no blockage scenario, the river erodes only the dam's outer edges. The solid line represents the initial water level, while the dashed line represents the raised water level.

debris flow materials may be carried downstream by the river flow and debris flow cannot move to the opposite bank. Once the volume is sufficient, debris flow has the potential to overcome the action of water flow and blocks the river. In addition, the parameters like ratio of debris flow height to river channel depth, confluent angle and characteristic particle size may also significantly impact the debris flow river blockage process. Although Eq. (8) has been successful in predicting the river blockage of the field cases featured here, prediction over a broader dataset remains essential to further assess and enhance the model's predictive capability. Due to the limitation of experimental conditions, our experiments showed viscous forces dominated debris-flow behavior, whereas natural cases indicate friction dominates. Therefore, a steeper flume and incorporate coarser particles (>20 mm) into the debris-flow mixture will be considered in the future study. Moreover, we did not study the process of debris flow dam break, which is also an important link of debris flow-induced river blockage hazard chain. These aspects will be refined in future studies.

5. Conclusions

This study addresses the mechanisms of river blockage by debris flows through physical flume experiments and comparisons with blockages by dry avalanches. Analysis was conducted on the flow deflection, dam formation, and outburst behavior. A Froude number–based criterion was developed to predict blockage outcomes, and validated using field data. The following conclusions can be obtained from this study:

(1) Debris flow deflection is less sensitive to river flow than dry avalanches. This is attributed to the characteristics of interstitial fluid, which reduce permeability and dispersion and maintain a compact flow structure, in contrast to the easily deflected dry avalanches.
(2) Outburst floods from debris flow dams are not abrupt. Hydrographs of debris flow dams exhibit smoother, more gradual water level changes, while dry avalanche dams tend to produce sharper peaks and sudden drops due to rapid breaching. These patterns reflect differences in dam geometry and breaching dynamics.
(3) The predictive criterion based on relative Froude numbers effectively distinguishes between blockage and no blockage scenarios for debris flows. The results also show that debris flows require lower momentum than dry avalanches to block rivers, confirming that landslide-based models cannot be directly applied to debris flows.

This study significantly investigated the different mechanisms of debris flow and dry avalanche blocking rivers and provided a new criterion to distinguish different river blockage modes which is helpful for early warning and mitigation of losses caused by debris flow blocking rivers. While the study demonstrates the effectiveness of a Froude-based predictive model, it assumes constant debris flow volume and river width. Future research should improve experimental conditions and explore how varying material volumes, channel widths, and additional parameters such as confluent angles and particle size distributions influence blockage outcomes. Moreover, the current model does not differentiate the degree of partial blockage nor simulate dam break processes—both of which are crucial for comprehensive hazard modeling and should be addressed in follow-up studies.

Notations

Q, W	Flow discharge in the main channel (L/s); water content of debris flow
$A, A_{df}, A_s, B, B_{df}, B_s$	Fitting parameters of debris flows and dry avalanches
$Fr, Fr_w, Fr_{df}, Fr_s, Fr^*$	Froude number; Froude number of river flow; Froude number of debris flow; Froude number of dry avalanche; and Froude number ratio
h, h_w, h_{df}, h_t	Depth (m); depth of river flow (m); depth of debris flow (m); depth of river flow at time t (m)
$L_1, L_2, L^*, L_1', L_2', b$	The longest distance of the deposit upstream from the center line (m); the longest distance downstream from the center line (m); deflection factor; upstream dimensionless distance; downstream dimensionless distance; the width of the tributary channel (m)
v, v_w, v_{df}	Velocity (m/s); velocity of river flow (m/s); velocity of debris flow (m/s)
g	The gravitational acceleration (m/s^2)
t, t^*	The real time of the tests (s); dimensionless time
N_{Bag}, N_{Sav}, N_{Fric}	Bagnold number; Savage number; Friction number
ρ, ρ_f, ρ_s	Density (kg/m^3); fluid density (kg/m^3); solid density (kg/m^3)
μ, μ_w	Interstitial fluid dynamic viscosity $(Pa \bullet s)$; dynamic viscosity of pure water $(Pa \bullet s)$
V_s, V_{fine}	Volume fraction of the solid particles; volume fraction of the interstitial fluid occupied by fines
θ	Channel inclination $(^\circ)$
δ	Characteristic size of the sediments (m)
$\dot{\gamma}$	Shear rate (s^{-1})

CRediT authorship contribution statement

Tianjia Zhou: Writing – review & editing, Writing – original draft, Methodology. **Gordon G.D. Zhou:** Writing – review & editing, Supervision, Methodology, Funding acquisition. **Kahlil F.E. Cui:** Writing – review & editing, Supervision, Methodology. **Hongwei Luo:** Writing – review & editing, Supervision, Methodology. **Xueqiang Lu:** Writing – review & editing, Supervision, Methodology. **Alessandro Pasuto:** Writing – review & editing. **Giulia Bossi:** Writing – review & editing.

Declaration of competing interest

The authors declare that they have no known competing financial interests or personal relationships that could have appeared to influence the work reported in this paper.

Acknowledgements

The authors acknowledge the financial support from the National Key R&D Program of China (2024YFE0104200), National Natural Science Foundation of China (Grant No. U24A20618), and Sichuan Science and Technology Program (2024NSFJQ0043).

Appendix

Table 2
Cases of blockage/no blockage collected from the literature and parameters of natural debris/ river flows.

NO.	Name and Location	Date	Debris flow				River				Mode	Data source
			v_{df} (m/s)	h_{df} (m)	θ_{df} (°)	Fr_{df}	v_w (m/s)	h_w (m)	θ_w (°)	Fr_w		
①	Peilong gully (94°56′00″E, 30°04′30″N)	1983.07.29	7.440	13.000	7.529	0.662	5.090	0.690	0.294	1.957	NB	(Cheng et al., 2005, 2007a, 2007b; Li et al., 2021)
②	Majingzi gully (102°23′26.14″E, 29°10′52.55″N)	2013.07.04	11.600	3.900	7.668	1.885	7.800	2.180	3.662	1.689	NB	(Ni et al., 2014; Liu et al., 2017)
③	Banzi gully (103°31′47.22″E, 31°24′27.53″N)	2019.08.20	4.740	2.100	10.758	1.054	5.400	5.000	0.917	0.771	NB	(Xiong et al., 2021; Wang et al., 2022)
④	Banzi gully (103°31′47.22″E, 31°24′27.53″N)	2023.06.26	8.340	2.000	11.640	1.903	5.400	1.987	0.917	1.224	NB	(Zhang et al., 2023; Chen et al., 2024b)
⑤	Wawa gully (102°03′27″E, 29°15′59″N)	2006.07.16	10.780	4.040	7.000	1.720	1.010	3.886	3.165	0.164	B	(Shi et al., 2008; Xie, 2024)
⑥	Mozi gully (102°12′29.53″E, 29°57′25.39″N)	2008.07.14	3.390	4.500	17.000	0.522	0.263	12.000	4.574	0.024	B	(Su, 2011)
⑦	Namasha (120°44′39.44″E, 23°19′39.49″N)	2009.08.08	35.700	1.210	17.800	10.624	11.100	5.920	1.200	1.457	B	(Chen et al. 2019)
⑧	Hou gully (102°22′30.06″E, 29°12′49.5″N)	2013.07.04	12.700	4.600	10.093	1.906	1.358	5.000	2.176	0.194	B	(Ni et al., 2014; Ge and Su, 2016; Liu et al., 2017)
⑨	Xiongjia gully (102°25′5.4″E, 29°09′27″N)	2013.07.04	12.400	3.800	7.125	2.040	2.345	5.800	2.176	0.311	B	(Ni et al., 2014; Song et al., 2016)
⑩	Mozi gully (102°12′29.53″E, 29°57′25.39″N)	2013.07.10	16.000	1.117	22.977	5.040	1.800	4.000	4.574	0.288	B	(Han et al., 2016)
⑪	Xiongmao gully (103°07′16.67″E, 30°58′29.19″N)	2016.07.26	3.130	1.500	5.54	0.818	1.300	3.654	1.432	0.217	B	(Liu, 2019)

Table 3
Debris flow dam and dammed lake parameters in cases that cause blockage/no blockage.

NO.	Name	Date	Dam				Lake			
			Volume ($\times 10^6 m^3$)	Height (m)	Length (m)	Width (m)	Volume ($\times 10^6 m^3$)	Length (km)	Width (m)	
①	Peilong Gully	1983.07.29	–	2–3	220	654	4.238	6.5	200	(Cheng et al., 2007b; Li et al., 2021)
②	Majingzi Gully	2013.07.04	0.175	5	275	330	–	–	–	(Ni et al., 2014)
③	Banzi Gully	2019.08.20	0.574	51.61	–	–	–	–	–	
④	Banzi Gully	2023.06.26	–	–	–	–	–	3.4	–	
⑤	Wawa Gully	2006.07.16	0.114	4	150	50	–	–	–	
⑥	Mozi Gully	2008.07.14	0.2	10	500	–	–	–	–	
⑦	Namasha	2009.08.08	6.667	22.6	606	1464	–	–	–	(Cheng et al., 2024)
⑧	Hou Gully	2013.07.04	0.415	6–8	300	80–100	–	–	–	
⑨	Xiongjia Gully	2013.07.04	0.115	4–7	150	64	–	–	–	
⑩	Mozi Gully	2013.07.10	0.064	20	100	–	–	–	–	
⑪	Xiongmao Gully	2016.07.26	–	–	120	30	–	–	–	

Note: "—" means there is no available data.

Data availability

Data will be made available on request.

References

Braun, A., Cuomo, S., Petrosino, S., Wang, X., Zhang, L., 2018. Numerical SPH analysis of debris flow run-out and related river damming scenarios for a local case study in SW China. Landslides 15, 535–550. https://doi.org/10.1007/s10346-017-0885-9.

Cabral, V., Reis, F., Veloso, V., Ogura, A., Zarfl, C., 2023. A multi-step hazard assessment for debris-flow prone areas influenced by hydroclimatic events. Eng. Geol. 313, 106961. https://doi.org/10.1016/j.enggeo.2022.106961.

Casagli, N., Ermini, L., Rosati, G., 2003. Determining grain size distribution of the material composing landslide dams in the Northern Apennines: sampling and processing methods. Eng. Geol. 69, 83–97. https://doi.org/10.1016/S0013-7952(02)00249-1.

Chen, K.-T., Chen, X.-Q., Hu, G.-S., Kuo, Y.-S., Huang, Y.-R., Shieh, C.-L., 2019a. Dimensionless assessment method of landslide dam formation caused by tributary debris flow events. Geofluids 2019, 1–14. https://doi.org/10.1155/2019/7083058.

Chen, K.-T., Chen, X.-Q., Niu, Z.-P., Guo, X.-J., 2019b. Early identification of river blocking induced by tributary debris flow based on dimensionless volume index. Landslides 16, 2335–2352. https://doi.org/10.1007/s10346-019-01221-8.
Chen, H., Ruan, H., Chen, J., Li, X., Yu, Y., 2022. Review of investigations on hazard chains triggered by river-blocking debris flows and dam-break floods. Front. Earth Sci. 10, 830044. https://doi.org/10.3389/feart.2022.830044.
Chen, Q., Song, D., Chen, X., Zhong, W., 2023. Visco-collisional scaling law of flow resistance and its application in debris-flow mobility. J. Geophys. Res. Earth Surf. 128, e2022JF006712. https://doi.org/10.1029/2022JF006712.
Chen, G., Chong, Y., Meng, X., Yang, Y., Yue, D., Jin, J., Bian, S., Shi, W., Zhang, Y., 2024. Experimental field study on the formation process of debris flow dam at channel confluence: implications for early identification of river blockage. Landslides 21, 1095–1108. https://doi.org/10.1007/s10346-023-02198-1.
Chen, H., Li, X., Chen, X., Ruan, H., Wang, T., 2024a. Contrast experiments on breaching characteristics of landslide dams and debris-flow dams. Can. Geotech. J., cgj-2023-0534 https://doi.org/10.1139/cgj-2023-0534.
Chen, H., Xiong, J., Zhao, W., Chen, J., Zhang, X., Ruan, H., Fang, C., Gong, L., 2024b. Catastrophic debris flow triggered by a June 26, 2023 rainstorm suggests the debris flow is still active 15 years after the Wenchuan seismic. Landslides 21, 1883–1897. https://doi.org/10.1007/s10346-024-02279-9.
Chen, H., Yu, Y., Jiang, Y., Wang, T., Chen, J., Ruan, H., 2024c. Study on the rapid prediction model of debris flow barrier dam volume and morphology under different river blocking modes. Landslides. https://doi.org/10.1007/s10346-024-02393-8.
Cheng, Z., Wu, J., Geng, X., 2005. Debris flow dam formation in Southeast Tibet. J. Mt. Sci. 2, 155–163. https://doi.org/10.1007/BF02918331.
Cheng, Z., Dang, C., Liu, J., Gong, Y., 2007a. Experiments of debris flow damming in Southeast Tibet. Earth Sci. Front. 14, 181–185. https://doi.org/10.1016/S1872-5791(08)60010-X.
Cheng, Z., Geng, X., Dang, C., Liu, J., 2007b. Modeling experiment of break of debris-flow dam. Wuhan Univ. J. Nat. Sci. 12, 588–594. https://doi.org/10.1007/s11859-006-0302-z.
Cheng, H., Hu, K., Liu, S., Zhang, X., Li, H., Zhang, Q., Ning, L., Gouli, M.R., Li, P., Yang, A., Zhao, P., 2024. A worldwide event-based debris-flow barrier dam dataset from 1800 to 2023. Earth Syst. Sci. Data Discuss. 2024, 1–43. https://doi.org/10.5194/essd-2024-382.
Chmiel, M., Walter, F., Wenner, M., Zhang, Z., McArdell, B.W., Hibert, C., 2021. Machine learning improves debris flow warning. Geophys. Res. Lett. 48. https://doi.org/10.1029/2020gl090874.
Choi, C.E., Au-Yeung, S.C.H., Ng, C.W.W., Song, D., 2015a. Flume investigation of landslide granular debris and water runup mechanisms. Géotech. Lett. 5, 28–32. https://doi.org/10.1680/geolett.14.00080.
Choi, C.E., Ng, C.W.W., Au-Yeung, S.C.H., Goodwin, S.R., 2015b. Froude characteristics of both dense granular and water flows in flume modelling. Landslides 12, 1197–1206. https://doi.org/10.1007/s10346-015-0628-8.
Costa, J.E., Schuster, R.L., 1988. The formation and failure of natural dams. Geol. Soc. Am. Bull. 100 (7), 1054–1068. https://doi.org/10.3133/ofr87392.
Cui, P., Zeng, C., Lei, Y., 2015. Experimental analysis on the impact force of viscous debris flow. Earth Surf. Process. Landf. 40, 1644–1655. https://doi.org/10.1002/esp.3744.
Cui, K.F.E., Zhou, G.G.D., Jing, L., 2021. Viscous effects on the particle size segregation in geophysical mass flows: insights from immersed granular shear flow simulations. J. Geophys. Res. Solid Earth 126, e2021JB022274. https://doi.org/10.1029/2021JB022274.
Dai, Z., Huang, Y., Cheng, H., Xu, Q., 2017. SPH model for fluid–structure interaction and its application to debris flow impact estimation. Landslides 14, 917–928. https://doi.org/10.1007/s10346-016-0777-4.
Dang, C., Cui, P., Cheng, Z., 2009. The formation and failure of debris flow-dams, background, key factors and model tests: case studies from China. Environ. Geol. 57, 1901. https://doi.org/10.1007/s00254-008-1479-6.
de Haas, T., Braat, L., Leuven, J.R.F.W., Lokhorst, I.R., Kleinhans, M.G., 2015. Effects of debris flow composition on runout, depositional mechanisms, and deposit morphology in laboratory experiments. J. Geophys. Res. Earth Surf. 120, 1949–1972. https://doi.org/10.1002/2015JF003525.
Dong, J.-J., 2011. The formation and breach of a short-lived landslide dam at Hsiaolin village, Taiwan — part I: post-event reconstruction of dam geometry. Eng. Geol. 123, 40–59. https://doi.org/10.1016/j.enggeo.2011.04.001.
Du, C., Yao, L., Shakya, S., Li, L., Sun, X., 2014. Damming of large river by debris flow: dynamic process and particle composition. J. Mt. Sci. 11, 634–643. https://doi.org/10.1007/s11629-012-2568-2.
Ge, Y., Su, F., 2016. Characteristics and causes of disastrous debris flows on July 4, 2013, in Shimian County, Sichuan, China. Int. J. Geosci. 07, 518–528. https://doi.org/10.4236/ijg.2016.74039.
Han, M., Hu, T., Wang, Y., Hong, M., 2016. Dynamics character and river-blocking analysis of narrow steep channels debris flow in Wenchuan earthquake region——illustrated with case of MoziI Gully along Duwen Freeway. J. Eng. Geol. 24, 559–568. https://doi.org/10.13544/j.cnki.jeg.2016.04.010 (in Chinese).
Hürlimann, M., McArdell, B.W., Rickli, C., 2015. Field and laboratory analysis of the runout characteristics of hillslope debris flows in Switzerland. Geomorphology 232, 20–32. https://doi.org/10.1016/j.geomorph.2014.11.030.
Hutter, K., Svendsen, B., Rickenmann, D., 1994. Debris flow modeling: a review. Contin. Mech. Thermodyn. 8, 1–35. https://doi.org/10.1007/BF01175749.
Iverson, R.M., 1997. The physics of debris flows. Rev. Geophys. 35, 245–296. https://doi.org/10.1029/97RG00426.
Iverson, R.M., Denlinger, R.P., 2001. Flow of variably fluidized granular masses across three-dimensional terrain: 1. Coulomb mixture theory. J. Geophys. Res. Solid Earth 106, 537–552. https://doi.org/10.1029/2000JB900329.
Iverson, R.M., Logan, M., LaHusen, R.G., Berti, M., 2010. The perfect debris flow? Aggregated results from 28 large-scale experiments. J. Geophys. Res. Earth Surf. 115, 2009JF001514. https://doi.org/10.1029/2009JF001514.
Jakob, M., Hungr, O., 2005. Debris-Flow Hazards and Related Phenomena, 1st edition. ed. Springer, Berlin; New York.
Jakob, M., McDougall, S., Santi, P. (Eds.), 2024. Advances in Debris-Flow Science and Practice. Springer International Publishing, Cham. https://doi.org/10.1007/978-3-031-48691-3.
Kim, N., Nakagawa, H., Kawaike, K., Zhang, H., 2019. Estimation of debris flow discharge coefficient considering sediment concentration. Int. J. Sediment Res. 34, 1–7. https://doi.org/10.1016/j.ijsrc.2018.05.003.
Kostynick, R., Matinpour, H., Pradeep, S., Haber, S., Sauret, A., Meiburg, E., Dunne, T., Arratia, P., Jerolmack, D., 2022. Rheology of debris flow materials is controlled by the distance from jamming. Proc. Natl. Acad. Sci. 119, e2209109119. https://doi.org/10.1073/pnas.2209109119.
Li, M.-H., Sung, R.-T., Dong, J.-J., Lee, C.-T., Chen, C.-C., 2011. The formation and breaching of a short-lived landslide dam at hsiaolin village, Taiwan — part II: simulation of debris flow with landslide dam breach. Eng. Geol. 123, 60–71. https://doi.org/10.1016/j.enggeo.2011.05.002.
Li, Y., Wang, B., Zhou, X., Gou, W., 2015. Variation in grain size distribution in debris flow. J. Mt. Sci. 12, 682–688. https://doi.org/10.1007/s11629-014-3351-3.
Li, Z., Zhou, F., Han, X., Chen, J., Li, Y., Zhai, S., Han, M., Bao, Y., 2021. Numerical simulation and analysis of a geological disaster chain in the Peilong valley, SE Tibetan Plateau. Bull. Eng. Geol. Environ. 80, 3405–3422. https://doi.org/10.1007/s10064-021-02109-5.
Liao, H., Yang, X., Lu, G., Tao, J., Zhou, J., 2019. Experimental study on the river blockage and landslide dam formation induced by rock slides. Eng. Geol. 261, 105269. https://doi.org/10.1016/j.enggeo.2019.105269.
Liu, Z., 2019. Research on development characteristics and control measures of Wolong Xiongmaogou in Sichuan Province (Master's Thesis). Chengdu University of Technology, Chengdu City. https://doi.org/10.26986/d.cnki.gcdlc.2019.000894 (in Chinese).
Liu, J., Lui, S., Meng, M., 2017. Study on disaster mechanism and characteristics of debris flow of Majingzi Gully in Shimian County of Sichuan Province. Subgrade Eng. 200–205. https://doi.org/10.13379/j.issn.1003-8825.2017.05.43 (in Chinese).
Liu, Y., Tang, Z., Huang, L., Stoesser, T., Fang, H., 2024. On the role of the froude number on flow, turbulence, and hyporheic exchange in open-channel flow through boulder arrays. Phys. Fluids 36, 95141. https://doi.org/10.1063/5.0222673.
Luo, H., Zhou, G.G.D., Lu, X., Cui, K.F.E., Zhao, Y., Xie, Y., Zhong, W., Zhou, J., Pasuto, A., 2025. Experimental investigation on the formation and failure of landslide dams considering the landslide mobility and river flow. Eng. Geol. 346, 107873. https://doi.org/10.1016/j.enggeo.2024.107873.
Ni, H., Zheng, W., Song, Z., Xu, W., 2014. Catastrophic debris flows triggered by a 4 July 2013 rainfall in Shimian, SW China: formation mechanism, disaster characteristics and the lessons learned. Landslides 11, 909–921. https://doi.org/10.1007/s10346-014-0514-9.
Nian, T., Wu, H., Li, D., Zhao, W., Takara, K., Zheng, D., 2020. Experimental investigation on the formation process of landslide dams and a criterion of river blockage. Landslides 17, 2547–2562. https://doi.org/10.1007/s10346-020-01494-4.
Ruan, H., Chen, H., Chen, X., Zhao, W., Chen, J., Wang, T., Jiang, Y., Wang, X., Li, Xiangning, Li, Xiao, Yu, Y., 2023. Modeling of breaching parameters for debris flow dams. J. Mt. Sci. 20, 2835–2851. https://doi.org/10.1007/s11629-023-8052-3.
Shen, W., Wang, D., He, S., Li, T., 2020. Numerical assessment of the impeding effect of check dams in the Hongchun debris flow gully, Sichuan Province, China. Bull. Eng. Geol. Environ. 79, 2833–2845. https://doi.org/10.1007/s10064-020-01755-5.
Shi, L., Chen, N., Yang, C., 2008. Debris flow activity characteristics and blocking up river mechanism in Wawa Valley Jiulong County Sichuan Province. Chin. J. Geol. Hazard Control. 16–21+48. https://doi.org/10.16031/j.cnki.issn.1003—8035.2008.02.01 (in Chinese).
Song, Z., Deng, R., Chen, Z., 2016. Analysis of motion process and accumulation zone characteristics of a typical debris flow blocking river case: a case study of the debris flow in Xiongjia Gully. J. Nat. Disasters 25, 74–80. https://doi.org/10.13577/j.jnd.2016.0109 (in Chinese).
Stancanelli, L.M., Lanzoni, S., Foti, E., 2014. Mutual interference of two debris flow deposits delivered in a downstream river reach. J. Mt. Sci. 11, 1385–1395. https://doi.org/10.1007/s11629-014-3051-z.
Stancanelli, L.M., Lanzoni, S., Foti, E., 2015. Propagation and deposition of stony debris flows at channel confluences. Water Resour. Res. 51, 5100–5116. https://doi.org/10.1002/2015WR017116.
Su, P., 2011. Debris flows in Mozi gully, China following the 2008 Wenchuan earthquake. Ital. J. Eng. Geol. Environ. 769–777. https://doi.org/10.4408/IJEGE.2011-03.B-084.
Swanson, F.J., Graham, R.L., Grant, G.E., 1985. Some effects of slope movements on river channels. Proc. Int. Symp. Eros. Debris Flow Disaster Prev. 273–278.
Tacconi Stefanelli, C., Segoni, S., Casagli, N., Catani, F., 2016. Geomorphic indexing of landslide dams evolution. Eng. Geol. 208, 1–10. https://doi.org/10.1016/j.enggeo.2016.04.024.
Takahashi, T., 2007. Debris flow: Mechanics, prediction and countermeasures. In: Balkema - Proceedings and Monographs in Engineering, Water and Earth Sciences, 1st Edition. ed. Taylor & Francis, Leiden.
Wang, T., Chen, X., Li, K., Chen, J., You, Y., 2018. Experimental study of viscous debris flow characteristics in drainage channel with oblique symmetrical sills. Eng. Geol. 233, 55–62. https://doi.org/10.1016/j.enggeo.2017.11.024.
Wang, D., You, Y., Li, D., Liu, J., Sun, H., Lv, X., Wang, Z., 2022. The river blockage characteristics of "8·20" large-scale debris flow and the hazard prediction in Banzi

gully in Miansi Town, Wenchuan County. Chin. J. Geol. Hazard Control 33, 58–66. https://doi.org/10.16031/j.cnki.issn.1003-8035.2022.01-07 (in Chinese).
Xie, Q., 2024. The Effects of Knickpoints on Erosion in Rapid Lift Region ——Take Hongba River for Example (Master's Thesis). Sichuan Agricultural University, Ya'an City. https://doi.org/10.27345/d.cnki.gsnyu.2024.001207 (in Chinese).
Xiong, J., Tang, C., Chen, M., Zhang, X., Shi, Q., Gong, L., 2021. Activity characteristics and enlightenment of the debris flow triggered by the rainstorm on 20 August 2019 in Wenchuan County, China. Bull. Eng. Geol. Environ. 80, 873–888. https://doi.org/10.1007/s10064-020-01981-x.
Yan, Y., Tang, H., Hu, K., Turowski, J.M., Wei, F., 2023. Deriving debris-flow dynamics from real-time impact-force measurements. J. Geophys. Res. Earth Surf. 128, e2022JF006715. https://doi.org/10.1029/2022JF006715.
Yu, B., Yang, C., Yu, M., 2022. Experimental study on the critical condition of river blockage by a viscous debris flow. Catena 213, 106198. https://doi.org/10.1016/j.catena.2022.106198.
Zeng, J., Zhao, Y., Zheng, J., Zhang, Y., Shi, P., Li, Y., Chen, G., Meng, X., Yue, D., 2024. Early identification of river blockage disasters caused by debris flows in the Bailong River Basin, China. Remote Sens 16, 1302. https://doi.org/10.3390/rs16071302.
Zhang, J., Cui, P., 2013. An empirical formula for suspended sediment delivery ratio of main river after confluence of debris flow. J. Mt. Sci. 10, 326–336. https://doi.org/10.1007/s11629-013-2519-6.
Zhang, X., Tie, Y., Ning, Z., Yang, C., Li, Z., Li, M., Liang, J., Lu, J., Lu, T., Guanghui, Li, Guo, Li, Xiang, B., 2023. Characteristics and activity analysis of the catastrophic "6•26" debris flow in the Banzi catchment, Wenchuan County of Sichuan Province. Hydrogeol. Eng. Geol. 50, 134–145. https://doi.org/10.16030/j.cnki.issn.1000-3665.202307003 (in Chinese).
Zhou, G.G.D., Ng, C.W.W., 2010. Dimensional analysis of natural debris flows. Can. Geotech. J. 47, 719–729. https://doi.org/10.1139/T09-134.
Zhou, G.G.D., Li, S., Song, D., Choi, C.E., Chen, X., 2019a. Depositional mechanisms and morphology of debris flow: physical modelling. Landslides 16, 315–332. https://doi.org/10.1007/s10346-018-1095-9.
Zhou, M., Zhou, G.G.D., Cui, K.F.E., Song, D., Lu, X., 2019b. Influence of inflow discharge and bed erodibility on outburst flood of landslide dam. J. Mt. Sci. 16, 778–792. https://doi.org/10.1007/s11629-018-5312-8.
Zhou, G.G.D., Cui, K.F.E., Jing, L., Zhao, T., Song, D., Huang, Y., 2020. Particle size segregation in granular mass flows with different ambient fluids. J. Geophys. Res. Solid Earth 125, e2020JB019536. https://doi.org/10.1029/2020JB019536.
Zou, Q., Cui, P., Jiang, H., Wang, J., Li, C., Zhou, B., 2020. Analysis of regional river blocking by debris flows in response to climate change. Sci. Total Environ. 741, 140262. https://doi.org/10.1016/j.scitotenv.2020.140262.